Computing steady-state solutions for a free boundary problem modeling tumor growth by Stokes equation

Wenrui Hao* Jonathan D. Hauenstein† Bei Hu‡

Timothy McCoy§ Andrew J. Sommese¶

September 25, 2011

Abstract

We consider a free boundary problem modeling tumor growth where the model equations include a diffusion equation for the nutrient concentration and the Stokes equation for the proliferation of tumor cells. For any positive radius R, it is known that there exists a unique radially symmetric stationary solution. The proliferation rate μ and the cell-to-cell adhesiveness γ are two parameters for characterizing "aggressiveness" of the tumor. We compute symmetry-breaking bifurcation branches of solutions by studying a polynomial discretization of the system. By tracking the discretized system, we numerically verified a sequence of μ/γ symmetry breaking bifurcation branches. Furthermore, we study the stability of both radially symmetric and radially asymmetric stationary solutions.

Keywords: Free boundary problems; Stationary solution; Stokes equation; Bifurcation; Stability; Homotopy continuation; Tumor growth

1 Introduction

Mathematical models of tumor growth, which consider the tumor tissue as a density of proliferating cells, have been developed and studied in many papers; see [1, 3, 5, 6, 7, 8, 9, 15, 18] and their references. These models treat tumor

*Department of Applied and Computational Mathematics and Statistics, University of Notre Dame, Notre Dame, IN 46556 (whao@nd.edu, www.nd.edu/∼whao). This author was supported by the Dunces Chair of the University of Notre Dame and NSF grant DMS-0712910.

†Department of Mathematics, Mailstop 3368, Texas A&M University, College Station, TX 77843 (jhauenst@math.tamu.edu, www.math.tamu.edu/∼jhauenst). This author was supported by Texas A&M University and NSF grant DMS-0915211 and DMS-1114336.

‡Department of Applied and Computational Mathematics and Statistics, University of Notre Dame, Notre Dame, IN 46556 (b1hu@nd.edu, www.nd.edu/∼b1hu).

§Department of Applied and Computational Mathematics and Statistics, University of Notre Dame, Notre Dame, IN 46556 (tmccoy@nd.edu).

¶Department of Applied and Computational Mathematics and Statistics, University of Notre Dame, Notre Dame, IN 46556 (sommese@nd.edu, www.nd.edu/∼sommese). This author was supported by the Duncan Chair of the University of Notre Dame and NSF grant DMS-0712910.

tissue as a porous medium described by Darcy's law. However, there are tumors for which the tissue is more naturally modeled as a fluid. For example, in the early stages of breast cancer, the tumor is confined to the duct of a mammary gland, which consists of epithelial cells, a meshwork of proteins, and mostly extracellular fluid. Several papers on ductal carcinoma in the breast use the Stokes equation in their mathematical models [10, 11, 12] with a focus on the radially symmetric case since tumors grown in vitro have a nearly spherical shape, it is important to determine whether these radially symmetric tumors are asymptotically stable. While tumors grown in vitro have a nearly spherical shape, tumors grown in vivo are usually not. It is therefore also interesting to study what will happen for the radially asymmetric tumors.

Let $\Omega(t)$ denote the tumor domain at time t, and p be the pressure within the tumor resulting from proliferation of the tumor cells. The density of the cells, c, depends on the concentration of nutrients, σ, and assuming that this dependence is linear, we may simply identify c with σ. We also assume the proliferation rate, S, depends linearly upon σ. That is,

$$\mathrm{div}\vec{v} = S = \mu(\sigma - \widetilde{\sigma}) \quad \text{in } \Omega(t), \tag{1}$$

where $\widetilde{\sigma} > 0$ is a threshold concentration and μ is the proliferation rate which expresses the "intensity" of the expansion or shrinkage. The first order Taylor expansion for the fully nonlinear model yields the linear approximation $\mu(\sigma - \widetilde{\sigma})$ used here.

If we assume that the consumption rate of nutrients is proportional to the concentration of the nutrients, then after normalization, σ satisfies

$$\sigma_t - \Delta\sigma = -\sigma \quad \text{in } \Omega(t) \;\text{ and }\; \sigma = 1 \quad \text{on } \partial\Omega(t). \tag{2}$$

Most tumor models assume that the tissue has the structure of a porous medium so that Darcy's law holds. In particular, $\vec{v} = -\nabla p$ where $\vec{v}$ is the velocity of the cells and p is the pressure. However, the tissue is modeled as a fluid in the current model. In this case, the stress tensor is given by $\sigma_{ij} = -p\delta_{ij} + 2\nu\Big(e_{ij} - \frac{1}{3}\bar{\Delta}\ \delta_{ij}\Big)$ where $p = -\frac{1}{3}\sum_{k=1}^{3}\sigma_{kk}$, ν is the viscosity coefficient, $e_{ij} = \frac{1}{2}\Big(\frac{\partial v_i}{\partial x_j} + \frac{\partial v_j}{\partial x_i}\Big)$ is the strain tensor, δ is the Kronecker delta and $\bar{\Delta} = \sum_{k=1}^{3} e_{kk} = \mathrm{div}\vec{v}$ is the dilation. If there are no body forces, then $\displaystyle\sum_{j=1}^{3}\frac{\partial\sigma_{ij}}{\partial x_j} = 0$ which can be written as the Stokes equation

$$-\nu\Delta\vec{v} + \nabla p - \frac{1}{3}\nu\nabla\mathrm{div}\vec{v} = 0 \quad \text{in } \Omega(t), \;\; t > 0. \tag{3}$$

Assuming that the strain tensor is continuous up to the boundary of the domain, we then obtain a boundary condition:

$$T\vec{n} = -\gamma\kappa\vec{n} \quad \text{on } \partial\Omega(t), \;\; t > 0, \tag{4}$$

where T is the stress tensor: $T = \nu(\nabla\vec{v} + (\nabla\vec{v})^T) - (p + \frac{2}{3}\nu \,\mathrm{div}\vec{v})I$ with components

$$T_{ij} = \nu\Big(\frac{\partial v_i}{\partial x_j} + \frac{\partial v_j}{\partial x_i}\Big) - \delta_{ij}\Big(p + \frac{2\nu}{3}\mathrm{div}\vec{v}\Big),$$

where $\vec{n}$ is the outward normal, κ is the mean curvature, and γ is the cell-to-cell adhesiveness constant.

The free boundary condition is given by the kinematic condition

$$V_n(t) = \vec{v}\cdot\vec{n} \quad \text{on } \partial\Omega(t). \tag{5}$$

Summarizing these equations, we obtain

$$\begin{cases} \sigma_t - \Delta\sigma + \sigma &= 0 & \text{in } \Omega(t) \\ -\Delta\vec{v} + \nabla p &= (\mu/3)\nabla(\sigma - \widetilde{\sigma}) & \text{in } \Omega(t) \\ \mathrm{div}\vec{v} &= \mu(\sigma - \widetilde{\sigma}) & \text{in } \Omega(t) \\ T(\vec{v},p)\vec{n} &= (-\gamma\kappa + \frac{2\nu}{3}\mu(1-\widetilde{\sigma}))\vec{n} & \text{on } \partial\Omega(t) \\ \sigma &= 1 & \text{on } \partial\Omega(t) \\ \vec{v}\cdot\vec{n} &= V_n & \text{on } \partial\Omega(t) \\ \int_{\Omega(t)} \vec{v}dx = 0 & , \quad \int_{\Omega(t)} \vec{v}\times\vec{x}dx = 0 & \end{cases} \tag{6}$$

where the last two conditions represent the choice of a coordinate system that excludes the six-dimensional kernel of (1), (3) and (4), which consists of rigid motions.

The steady state fluid-like tumor system is [13]:

$$\begin{cases} -\Delta\sigma + \sigma &= 0 & \text{in } \Omega \\ -\Delta\vec{v} + \nabla p &= (\mu/3)\nabla(\sigma - \widetilde{\sigma}) & \text{in } \Omega \\ \mathrm{div}\vec{v} &= \mu(\sigma - \widetilde{\sigma}) & \text{in } \Omega \\ T(\vec{v},p)\vec{n} &= (-\gamma\kappa + \frac{2\nu}{3}\mu(1-\widetilde{\sigma}))\vec{n} & \text{on } \partial\Omega \\ \sigma &= 1 & \text{on } \partial\Omega \\ \vec{v}\cdot\vec{n} &= 0 & \text{on } \partial\Omega \\ \int_{\Omega} \vec{v}dx = 0 & , \quad \int_{\Omega} \vec{v}\times\vec{x}dx = 0 & \end{cases} \tag{7}$$

where $T(\vec{v},p)\vec{n} = (\nabla\vec{v})^T + \nabla\vec{v} - pI$ with I the 3×3 identity matrix.

In [13], it is proved that there exists a unique radially symmetric solution with free boundary $r = R$ for any given positive number R. For a sequence $\mu/\gamma = M_n(R)$ there exist symmetry-breaking bifurcation branches of solutions with boundary $r = R + \epsilon Y_{n,0}(\theta) + O(\epsilon^2)$ (n even ≥ 2) for small $|\epsilon|$, where $Y_{n,0}$ is the spherical harmonic of mode $(n, 0)$. Note that these results are valid only in a small neighborhood of the bifurcation branching point. In this paper, we use the numerical method presented in [17] to find the radially asymmetric solutions as the parameters *go beyond this small neighborhood*, e.g., Figure 4. Compare with the system in [17], this system has more variables and increased complexity when using a similar discretization scheme. The comparison of the complexity is shown in Table 1 and thus the extension of our method is not a trivial extension; as a matter of fact, this required us to implement and use parallel differentiation and a sparse linear solver in order to perform the large-scale numerical computations needed for the method developed in [17]. We will discuss the details in the next section. Just like the system in [17], our numerical bifurcation value matches the theoretical value very well as shown in Table 2.

2 Discretization

We use the floating grid mentioned in [16, 17] and third order finite difference scheme for the spherical coordinate expression of the radially symmetric stationary solution of system (7) presented in [13]. The formula for the operators in the system in spherical coordinates is deduced in the Appendix. The values $(\sigma, \vec{v}, p)$ in the small neighborhood of a bifurcation point obtained in [13] via linearization are

$$\begin{cases} \sigma = \sigma_s + \epsilon\sigma_1 + O(\epsilon^2), & \sigma_1 = -(\sigma_s)_r(R)\frac{I_{l+1/2}(r)}{r^{1/2}}\frac{R^{1/2}}{I_{l+1/2}(R)}Y_{l,0}(\theta,\phi) \\ p = p_s + \epsilon p_1 + O(\epsilon^2), & p_1 = \frac{4\mu}{3}\sigma_1 + p_{l,0}(r)Y_{l,0}(\theta,\phi) \\ \vec{v} = \vec{v}_s + \epsilon\vec{v}_1 + O(\epsilon^2), & \vec{v}_1 = \vec{a} + \vec{b} \times \vec{x} + H_1(r)Y_{l,0}\vec{e}_r + H_2(r)\nabla_\omega Y_{l,0}(\theta,\phi) \end{cases},$$

where $Y_{l,0}(\theta, \phi)$ is the spherical harmonic function, which satisfies $Y_{l,0}(\theta, \phi) = Y_{l,0}(\pi - \theta, \phi)$, and $H_1(r), H_2(r)$ are functions of r (see [13] for detail). Then σ and p are symmetric with respect to $\frac{\pi}{2}$. We note that $\vec{v}$ can be written as $v_r\vec{e}_r + v_\theta\vec{e}_\theta + v_\phi\vec{e}_\phi$, that $\nabla_\omega = \frac{1}{\sin(\theta)}\frac{\partial}{\partial\theta}\left(\sin(\theta)\frac{\partial}{\partial\theta}\right) + \frac{1}{\sin^2\theta}\frac{\partial^2}{\partial\phi^2}$, and

$$\begin{cases} \sigma(\theta) = \sigma(\pi - \theta) \\ p(\theta) = p(\pi - \theta) \\ v_r(\theta) = v_r(\pi - \theta) \qquad \text{for } \theta \in \left[0, \frac{\pi}{2}\right] \\ v_\phi(\theta) = 0 \\ -v_\theta(\theta) = v_\theta(\pi - \theta) \end{cases}$$

for the bifurcation branch of $M_n(R)$, where n is an even number. In particular, due to this symmetry, we can construct the grid points on one-eighth of the domain and then extend using symmetry to yield solutions to the whole domain.

3 Bifurcation of $M_n(R)$

Using the floating grid and third order scheme presented in [16, 17], we setup a discretization of the system (7) yielding a polynomial system. Due to the complexity of this polynomial system, it required more computational power than the tumor systems in [16, 17]. We used Bertini [2] to handle this polynomial system running on a Xeon 5410 processor using 64-bit Linux. In order to better handle this large-scale problem using Bertini, we implemented parallel differentiation and a sparse linear algebra solver based on BLAS [4] in Bertini. Table 1 compares the number of variables and time needed to track the discretized polynomial systems along the radially symmetric branch between porous media

Tumor Model	N_θ	N_R	Number of variables	time
porous media in [17]	16	30	575	8m24s
	32	60	1135	1h30m
fluid-like	16	30	1008	7h28m
	32	60	3938	26h34m

Table 1: Comparison of polynomial system solving times

n	formula [13]	numerical value
M_4	0.47481	0.47494
M_6	0.47629	0.47702

Table 2: Comparison of the numerical values of μ_n with the actual value for a radius of $R = 12.5$

tumor model and fluid-like tumor model. In this table, N_θ and N_R denote the number of grid points in the angular and radial directions, respectively.

The system is parameterized by μ and γ, which characterize the "aggressiveness" of the tumor. It is known [13] that there exists a unique radially symmetric solution with any given μ. When we are tracking the radially symmetric solutions along the parameter μ with $\gamma = 1$, the Jacobian will become singular at μ_n where there exists a bifurcation. Starting from a radially symmetric solution and using parameter continuation with respect to μ, we are able to compute the value of M_n numerically. Figure 1 plots the condition number of radially symmetric solutions for different μ ranging between $\mu = 0.47$ and $\mu = 0.48$ with $R = 12.5$. We note that there are two bifurcations in the figure, namely $\mu = M_4$ and $\mu = M_6$, respectively. Table 2 compares the numerically computed values of M_n with the values of M_n given by the symbolic formulas derived in [13].

The radially asymmetric solutions along the bifurcation branches are even more interesting. We found that the double precision arithmetic in Matlab was unable to accurately compute the tangent directions at μ_n. This stems from the fact that the Jacobian matrix is singular at μ_n and has condition number around 10^9 even at values of μ where it is nonsingular. By using multiprecision arithmetic implemented in Bertini [2], we were able to compute the tangent directions which agreed with the symbolic formulas derived in [14]. Upon computing the tangent direction, we utilized parameter continuation to track the radially asymmetric solution branches passing through the values of M_4 and M_6 computed above. Figure 2 shows the solution behavior of these branches which were computed using $N_R = 60$ grid points in the radial direction and $N_\theta = 32$ grid points in the angular direction. The function $\epsilon(\theta)$ in this figure is defined in [17] allowing us to plot the branches. By looking at Figure 2, we see that there are three intersections. The two intersection, denoted M_U and M_L in Figure 2 are self-intersections which arise simply by the choice of the projection since the corresponding nonradial solutions as these points are distinct. The intersection denoted $M_{\text{nonradial}}$ in Figure 2 is indeed a nonradial bifurcation. To demonstrate

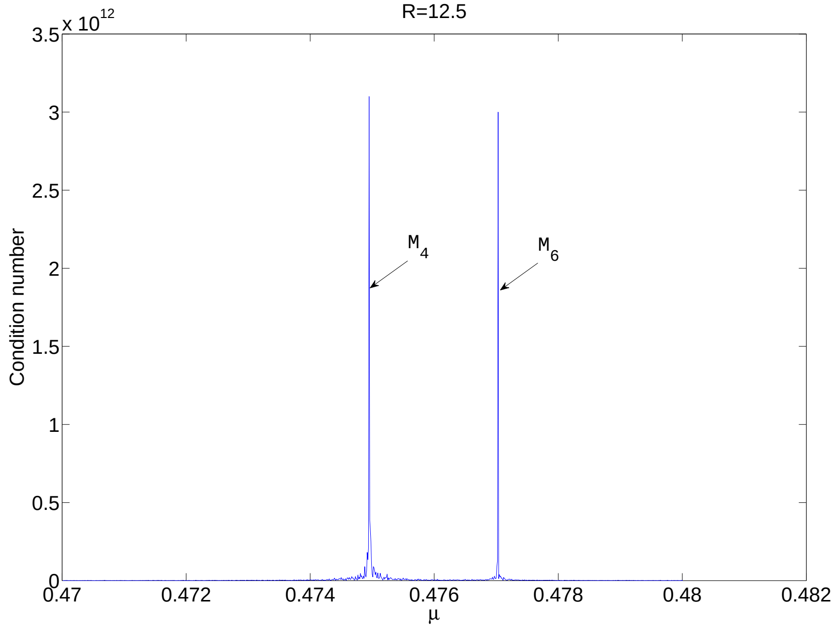

Figure 1: Condition Number of the radially symmetric solution vs. μ

this, Figure 3 plots the condition number along this path and clearly shows a bifurcation corresponding to the point $M_{\text{nonradial}}$. Figure 4 plots two nonradial solutions lying on the M_4 and M_6 branches, respectively.

4 Homotopy continuation of M_n to R

For the porous medium tissue model, the smallest value of μ/γ which generates protrusions is $M_2(R)$. At this point, the tumor will have just three protrusions independent of the value of R. However, in the case of a fluid-like tissue, [14] shows that the smallest value of μ/γ which generates protrusions is $M_{n*}(R)$, where n^* depends on R. Therefore, one natural question is to determine the values of R where n^* changes.

Since the value of $M_n(R)$ corresponds with a singular solution of a polynomial system, we use deflation to construct a new polynomial system which allows us to track along the path $M_n(R)$ parameterized by R. Let $f(x, \mu)$ denote the discretized polynomial system, where x^* corresponds to the numerical solution $(\sigma, p, \vec{v})$ at the bifurcation point μ^* of interest. Let $Jf(x, \mu)$ be the Jacobian matrix of f at x. Since the Jacobian is rank deficient, it has nonzero null vectors. One step of the deflation process adds polynomials to f to yield a

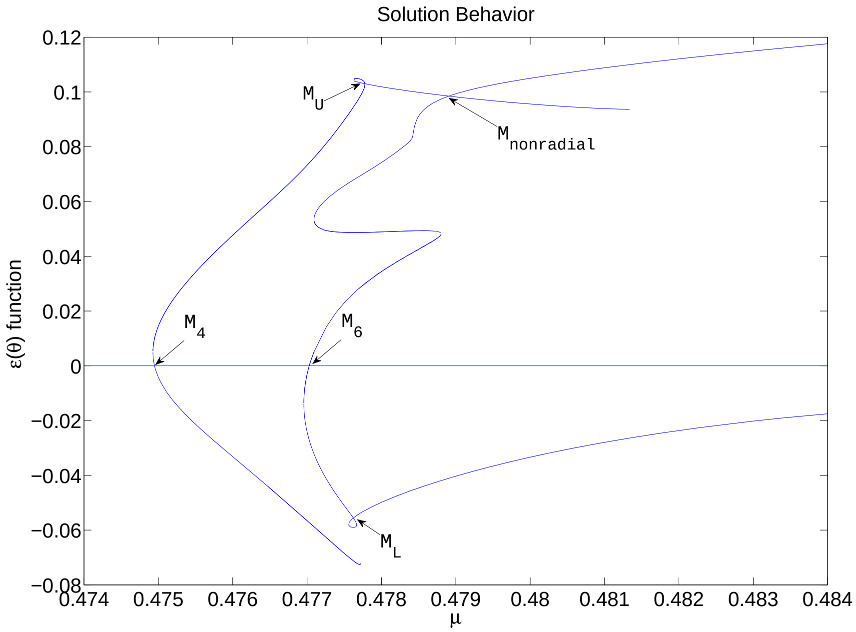

Figure 2: Solution Behavior

general element in this null space, namely the polynomial system

$$g(x, \mu, \xi) = \begin{bmatrix} f(x, \mu) \\ Jf(x, \mu)\xi \\ \mathcal{L}(\xi) \end{bmatrix}$$

where $\mathcal{L}(\xi)$ is a general linear system so that there is a unique value of ξ such that $g(x^*, \mu^*, \xi) = 0$. Using this augmented polynomial system, we can track a bifurcation value M_n as R varies. Figure 5 plots the value of M_4 with respect to R along with the numerical error. At the values R^* where n^* changes, the solution (x, μ, ξ) is singular, that is, the Jacobian matrix of $g(x, \mu, \xi)$ is rank deficient. Figure 6 plots the condition number of $Jg(x, \mu, \xi)$ with respect to R. This computation yields a numerical value of $R^* = 12.8778$.

5 Linear stability

We now turn our attention to the numerical determination of solution stability. In order to check linear stability, we rewrite (6) as

$$u_t = F(u, \mu, \widetilde{\sigma}, \gamma),$$

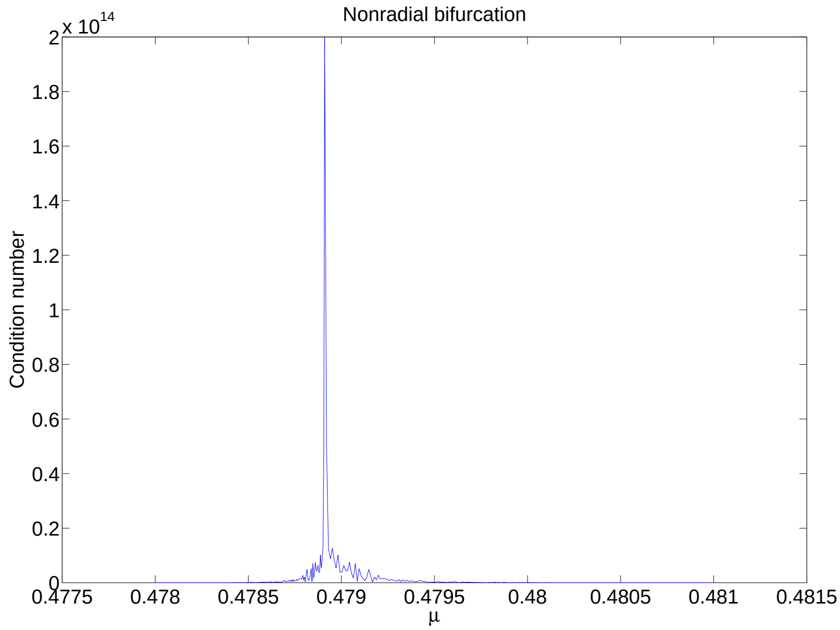

Figure 3: Nonradial bifurcation

where $u = (r, \sigma, p, \vec{v})$, r is the function of the angle θ describing the boundary and $F(u, \mu, \widetilde{\sigma}, \gamma)$ represents the steady state system (7). The linearization of the system (6) gives

$$u(t) = u_0 + \epsilon u_1(t) + O(\epsilon^2), \tag{8}$$

where u_0 is the steady state solution. Substituting (8) into (6), we have

$$\begin{aligned} & \left(u_0 + \epsilon u_1(t) + O(\epsilon^2)\right)_t = F(u_0 + \epsilon u_1(t) + O(\epsilon^2), \mu, \widetilde{\sigma}, \gamma) \\ \Rightarrow \quad & (u_0)_t + \epsilon(u_1)_t + O(\epsilon^2) = F(u_0, \mu, \widetilde{\sigma}, \gamma) + JF(u_0, \mu, \widetilde{\sigma}, \gamma)u_1\epsilon + O(\epsilon^2) \\ \Rightarrow \quad & (u_1)_t = JF(u_0, \mu, \widetilde{\sigma}, \gamma)u_1, \end{aligned} \tag{9}$$

where $JF(u_0, \mu, \widetilde{\sigma}, \gamma)$ is the Jacobian of $F(u, \mu, \widetilde{\sigma}, \gamma)$ at u_0. Let U_1^n denote the numerical approximation of $u_1(n\tau)$, where τ is the time step size. Then the discretization of (9) leads to

$$U_1^{n+1} = (I - JF(u_0, \mu, \widetilde{\sigma}, \gamma)\tau)^{-1} U_1^n \doteq AU_1^n,$$

where I is the identity matrix. This process transfers the linear stability to the spectrum of A. Let $|\rho(A)|$ denote the maximum of the absolute values of the

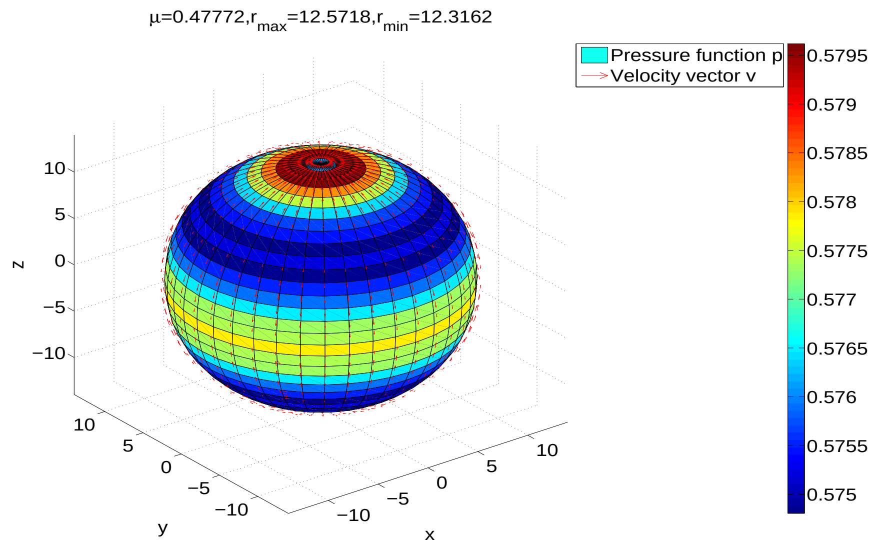

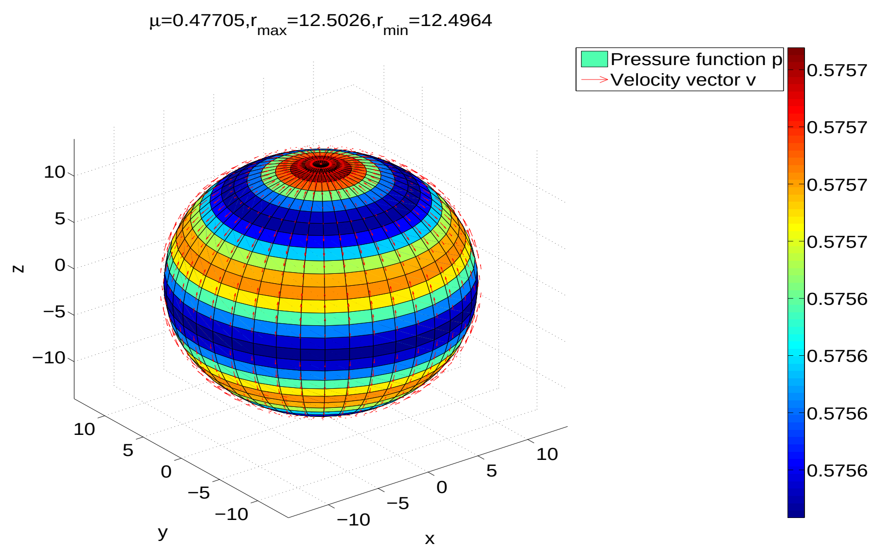

Figure 4: Radially asymmetric solutions

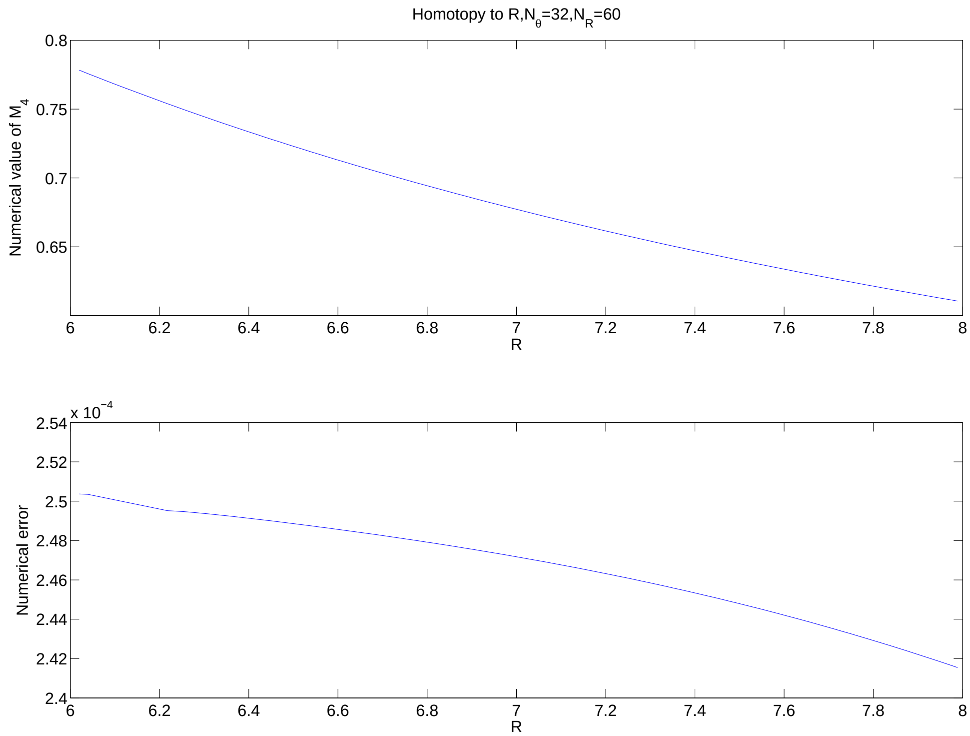

Figure 5: Homotopy of M_4

eigenvalues of A. If $|\rho(A)| < 1$, then $\|U_1^n\| \to 0$ yielding a stable system. The system is unstable if $|\rho(A)| > 1$. Continuing with the working example described in Section 3, namely $R = 12.5$, we computed the eigenvalues of A for different values of μ along the radially asymmetric solution branches to determine the stability which are displayed in Table 3. We note that "U" and "L" represent the "upper" and "lower" branches, respectively.

Table 3 shows that the solution is unstable even before the parameter μ reaches its first bifurcation point. This is in contrast with tumors growing in porous media environment where spherical instability occurs only when μ reaches the first bifurcation point. Moreover, all of the nonradial solutions computed are unstable while there are some stable nonradial solutions for a porous tumor [17].

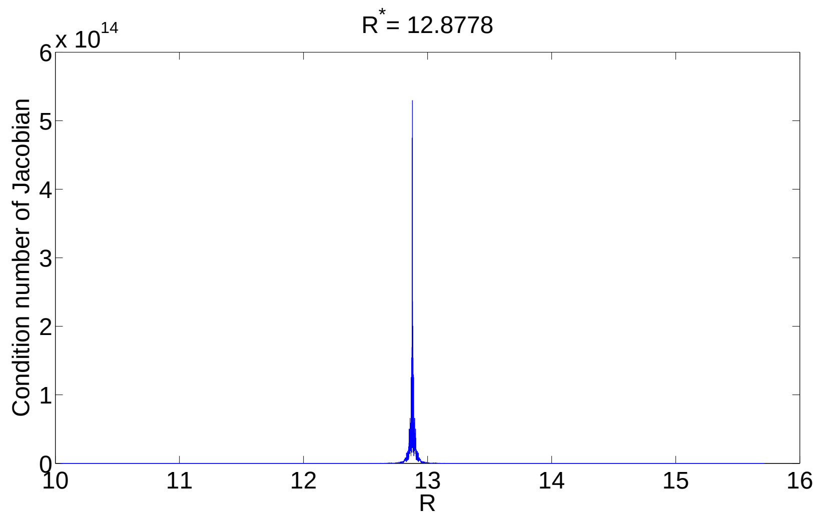

Figure 6: Condition number of $Jg(x, \mu, \xi)$ v.s. R

Table 3: Maximum eigenvalue for different values of μ

Radial branch	
μ	$\|\rho(A)\|$
1e-2	0.99865
5e-2	0.99990
1e-1	0.99999
2e-1	1.00032
3e-1	1.00012
4e-1	1.00049
5e-1	1.00148
6e-1	1.00638
8e-1	1.01846
1	1.09861

M_4 nonradial branch	
μ	$\|\rho(A)\|$
4.75766e-1U	1.00013
4.76641e-1U	1.00026
4.78324e-1U	1.00034
4.79012e-1U	1.00057
4.82764e-1U	1.00106
4.75766e-1L	1.00010
4.76000e-1L	1.00017
4.76290e-1L	1.00022
4.77101e-1L	1.00027
4.77629e-1L	1.00032

M_6 nonradial branch	
μ	$\|\rho(A)\|$
4.76956e-1U	1.00013
4.77128e-1U	1.00014
4.77297e-1U	1.00017
4.78802e-1U	1.00024
4.79208e-1U	1.00039
4.77093e-1L	1.00014
4.78053e-1L	1.00267
4.78727e-1L	1.00462
4.82026e-1L	1.00983
4.84000e-1L	1.01472

Acknowledgement

The authors would like to thank the Notre Dame Center for Research Computing (crc.nd.edu) for their help. Not only for helping maintain our group's computer cluster, but for providing access to a high memory node during the period when we were parallelizing the differentiation code in Bertini.

References

[1] J. A. Adam and S. A. Maggelakis, Diffusion regulated growth characteristics of a spherical prevascular carcinoma, *Bull. Math. Biol.*, Vol. 52, pp. 549–582. (1990)

[2] D.J. Bates, J.D. Hauenstein, A.J. Sommese, and C.W. Wampler, Bertini: Software for numerical algebraic geometry. *Available at www.nd.edu/∼sommese/bertini.*

[3] N. Britton and M.A.J. Chaplain, A qualitative analysis of some models of tissue growth, *Math. Biosci.*, Vol. 113, pp. 77–89, (1993).

[4] Sparse Basic Linear Algebra Subprograms (BLAS) Library, *http://math.nist.gov/spblas/.*

[5] H.M. Byrne, The importance of intercellular adhesion in the development of carcinomas, *IMA J. Math. Appl. Med. Biol.*, Vol. 14, pp. 305–323, (1997).

[6] H.M. Byrne, A weakly nonlinear analysis of a model of avascular solid tumor growth, *J. Math. Biol.*, Vol. 39, pp. 59–89, (1999).

[7] H.M. Byrne and M.A.J. Chaplain, Growth of nonnecrotic tumors in the presence and absence of inhibitors, *Math. Biosci.*, Vol. 130, pp. 151–181, (1995).

[8] H.M. Byrne and M.A.J. Chaplain, Modelling the role of cell-cell adhesion in the growth and development of carcinomas, *Mathl. Comput. Modelling*, Vol. 12, pp. 1–17, (1996).

[9] M.A.J. Chaplain, The development of a spatial pattern in a model for cancer growth, *Experimental and Theoretical Advances in Biological Pattern Formation* (H.G. Othmer, P.K. Maini, and J.D. Murray, eds), Plenum Press, pp. 45–60, (1993).

[10] S.J.H. Franks, H.M. Byrne, J.C.E. Underwood and C.E. Lewis, Biological inferences from a mathematical model of comedo ductal carcinoma in situ of the breast, *J. Theoretical Biology* Vol. 232, pp. 523–543, (2005).

[11] S.J.H. Franks, H.M. Byrne, J.P. King, J.C.E. Underwood and C.E. Lewis, Modelling the early growth of ductal carcinoma in situ of the brest, *J. Math. Biology*, Vol. 47, pp. 424-452. (2003)

[12] S.J.H. Franks, H.M. Byrne, J.P. King, J.C.E. Underwood and C.E. Lewis, Modelling the growth of ductal carcinoma in situ, *Mathematical Medicine & Biology*, Vol. 20, pp. 277–308, (2003).

[13] A. Friedman and B. Hu, Bifurcation for a free boundary problem modeling tumor growth by stokes equation *SIAM J. Math. Anal.*, Vol. 30, No. 1, pp.174–194, (2006).

[14] A. Friedman and B. Hu, Bifurcation from stability to instability for a free boundary problem modeling tumor growth by stokes equation, *J. Math. Anal. Appl.* Vol. 207, pp. 643–664, (2007).

[15] H. P. Greenspan, On the growth of cell culture and solid tumors, *J. Theoret. Biol.*, Vol. 56, pp. 229–242, (1976).

[16] W. Hao, J.D. Hauenstein, B. Hu, Y. Liu, A.J. Sommese and Y.-T. Zhang, Bifurcation for a free boundary problem modeling the growth of a tumor with a necrotic core, *Nonl. Anal.: Real Worl. Appl.*, to appear.

[17] W. Hao, J.D. Hauenstein, B. Hu and A.J. Sommese, A three-dimensional steady-state tumor system, *Appl. Math. Comp.*, to appear.

[18] D.L.S. McEwain and L.E. Morris, Apoptosis as a volume loss mechanism in mathematical models of solid tumor growth, *Math. Biosci.*, Vol. 39, 147–157, (1978).

Appendix: Operators under the spherical coordinate

We use the notation $\vec{e_r}, \vec{e_\theta}, \vec{e_\phi}$ for the unit normal vectors in the r, θ, ϕ directions, respectively; here $0 \leq r \leq \infty$, $0 \leq \theta \leq \pi$, $0 \leq \phi \leq 2\pi$. Then, written in Cartesian coordinates in $\mathbb{R}^3$,

$$\begin{aligned}
\vec{e}_r &= \vec{e}_1 \sin\theta\cos\phi + \vec{e}_2 \sin\theta\sin\phi + \vec{e}_3\cos\theta, \\
\vec{e}_\theta &= \vec{e}_1 \cos\theta\cos\phi + \vec{e}_2 \sin\theta\sin\phi + \vec{e}_3\cos\theta, \\
\vec{e}_\phi &= -\vec{e}_1 \sin\phi + \vec{e}_2\cos\phi,
\end{aligned}$$

where $(\vec{e}_1, \vec{e}_2, \vec{e}_3)$ is the standard basis in $\mathbb{R}^3$ in Cartesian coordinates.

The gradient of the vector $\nabla\vec{v}$, where $\vec{v} = (v_r, v_\theta, v_\phi)^T = v_r\vec{e}_r + v_\theta\vec{e}_\theta + v_\phi\vec{e}_\phi$, is given by

$$\nabla\vec{v} = \nabla v_r \otimes \vec{e}_r + \nabla v_\theta \otimes \vec{e}_\theta + \nabla v_\phi \otimes \vec{e}_\phi + v_r\nabla\vec{e}_r + v_\theta\nabla\vec{e}_\theta + v_\phi\nabla\vec{e}_\phi. \qquad (10)$$

In polar spherical coordinates, the gradient of a function f has the following form:

$$\nabla f = \frac{\partial f}{\partial r}\vec{e}_r + \frac{1}{r\sin\theta}\frac{\partial f}{\partial\phi}\vec{e}_\phi + \frac{1}{r}\frac{\partial f}{\partial\theta}\vec{e}_\theta.$$

Then, we can deduce the each term of (10) as follows,

$$
\begin{aligned}
\nabla v_r \otimes \vec{e}_r &= \left(\frac{\partial v_r}{\partial r}\vec{e}_r + \frac{1}{r\sin\theta}\frac{\partial v_r}{\partial \phi}\vec{e}_\phi + \frac{1}{r}\frac{\partial v_r}{\partial \theta}\vec{e}_\theta \right) \otimes \vec{e}_r \\
&= \frac{\partial v_r}{\partial r}\vec{e}_r \otimes \vec{e}_r + \frac{1}{r\sin\theta}\frac{\partial v_r}{\partial \phi}\vec{e}_\phi \otimes \vec{e}_r + \frac{1}{r}\frac{\partial v_r}{\partial \theta}\vec{e}_\theta \otimes \vec{e}_r \\
\nabla v_\theta \otimes \vec{e}_\theta &= \frac{\partial v_\theta}{\partial r}\vec{e}_r \otimes \vec{e}_\theta + \frac{1}{r\sin\theta}\frac{\partial v_\theta}{\partial \phi}\vec{e}_\phi \otimes \vec{e}_\theta + \frac{1}{r}\frac{\partial v_\theta}{\partial \theta}\vec{e}_\theta \otimes \vec{e}_\theta \\
\nabla v_\phi \otimes \vec{e}_\phi &= \frac{\partial v_\phi}{\partial r}\vec{e}_r \otimes \vec{e}_\phi + \frac{1}{r\sin\theta}\frac{\partial v_\phi}{\partial \phi}\vec{e}_\phi \otimes \vec{e}_\phi + \frac{1}{r}\frac{\partial v_\phi}{\partial \theta}\vec{e}_\theta \otimes \vec{e}_\phi \\
v_r \nabla \vec{e}_r &= v_r \left(\frac{\partial \vec{e}_r}{\partial r}\vec{e}_r + \frac{1}{r\sin\theta}\frac{\partial \vec{e}_r}{\partial \phi}\vec{e}_\phi + \frac{1}{r}\frac{\partial \vec{e}_r}{\partial \theta}\vec{e}_\theta \right) \\
&= \frac{v_r}{r}(\vec{e}_\phi \otimes \vec{e}_\phi + \vec{e}_\theta \otimes \vec{e}_\theta) \\
v_\theta \nabla \vec{e}_\theta &= \frac{v_\theta}{r}(\cot\theta \vec{e}_\phi \otimes \vec{e}_\phi - \vec{e}_r \otimes \vec{e}_\theta) \\
v_\phi \nabla \vec{e}_\phi &= -\frac{v_\phi}{r}(\cot\theta \vec{e}_\theta \otimes \vec{e}_\phi + \vec{e}_r \otimes \vec{e}_\phi)
\end{aligned}
$$

Therefore, we summarize the gradient of velocity as

$$
\nabla \vec{v} = \begin{pmatrix} \frac{\partial v_r}{\partial r}, & \frac{1}{r}\frac{\partial v_r}{\partial \theta}, & \frac{1}{r\sin\theta}\frac{\partial v_r}{\partial \phi} \\ \frac{\partial v_\theta}{\partial r} - \frac{v_\theta}{r}, & \frac{1}{r}\frac{\partial v_\theta}{\partial \theta} + \frac{v_r}{r}, & \frac{1}{r\sin\theta}\frac{\partial v_\theta}{\partial \phi} \\ \frac{\partial v_\phi}{\partial r} - \frac{v_\phi}{r}, & \frac{1}{r}\frac{\partial v_\phi}{\partial \theta} - \frac{\cot\theta}{r}v_\phi, & \frac{1}{r\sin\theta}\frac{\partial v_\phi}{\partial \phi} + \frac{v_r}{r} + \frac{\cot\theta}{r}v_\theta \end{pmatrix}.
$$

A vector Laplacian can be defined for a vector $\vec{v}$ by

$$
\Delta \vec{v} = \nabla(\nabla \cdot \vec{v}) - \nabla \times (\nabla \times \vec{v}).
$$

Moreover, the curl $\nabla \times \vec{v}$ under spherical coordinates is given by

$$
\nabla \times \vec{v} = \frac{\vec{e}_r}{r\sin\theta}\left[\frac{\partial}{\partial \theta}(v_\phi \sin\theta) - \frac{\partial v_\theta}{\partial \phi}\right] + \frac{\vec{e}_\theta}{r\sin\theta}\left[\frac{\partial v_r}{\partial \phi} - \sin\theta\frac{\partial}{\partial r}(r v_\phi)\right] + \frac{\vec{e}_\phi}{r}\left[\frac{\partial}{\partial r}(r v_\theta) - \frac{\partial v_r}{\partial \theta}\right].
$$

Thus, the Laplacian of velocity can be expressed as

$$
\Delta \vec{v} = \begin{pmatrix} \frac{1}{r}\frac{\partial^2 (r v_r)}{\partial r^2} + \frac{1}{r^2}\frac{\partial^2 v_r}{\partial \theta^2} + \frac{1}{r^2\sin^2\theta}\frac{\partial^2 v_r}{\partial \phi^2} + \frac{\cot\theta}{r^2}\frac{\partial v_r}{\partial \theta} - \frac{2}{r^2}\frac{\partial v_\theta}{\partial \theta} - \frac{2}{r^2\sin\theta}\frac{\partial v_\phi}{\partial \phi} - \frac{2v_r}{r^2} - \frac{2\cot\theta}{r^2}v_\theta \\ \frac{1}{r}\frac{\partial^2 (r v_\theta)}{\partial r^2} + \frac{1}{r^2}\frac{\partial^2 v_\theta}{\partial \theta^2} + \frac{1}{r^2\sin^2\theta}\frac{\partial^2 v_\theta}{\partial \phi^2} + \frac{\cot\theta}{r^2}\frac{\partial v_\theta}{\partial \theta} - \frac{2}{r^2}\frac{\cot\theta}{\sin\theta}\frac{\partial v_\phi}{\partial \phi} + \frac{2}{r^2}\frac{\partial v_r}{\partial \theta} - \frac{1}{r^2\sin^2\theta}v_\theta \\ \frac{1}{r}\frac{\partial^2 (r v_\phi)}{\partial r^2} + \frac{1}{r^2}\frac{\partial^2 v_\phi}{\partial \theta^2} + \frac{1}{r^2\sin^2\theta}\frac{\partial^2 v_\phi}{\partial \phi^2} + \frac{\cot\theta}{r^2}\frac{\partial v_\phi}{\partial \theta} + \frac{2}{r^2\sin\theta}\frac{\partial v_r}{\partial \phi} + \frac{2\cot\theta}{r^2\sin\theta}\frac{\partial v_\theta}{\partial \phi} - \frac{1}{r^2\sin^2\theta}v_\phi \end{pmatrix}.
$$